Journal of Hazardous Materials 187 (2011) 113–121

Contents lists available at ScienceDirect

Journal of Hazardous Materials

journal homepage: www.elsevier.com/locate/jhazmat

Modeling the operation of a three-stage fluidized bed reactor for removing CO_2 from flue gases

C.R. Mohanty[a], B.C. Meikap[b,c,*]

[a] Department of Civil Engineering, Veer Surendra Sai University of Technology, Burla, India
[b] School of Chemical Engineering, Howard College Campus, University of Kwazulu-Natal (UKZN), King George Avenue, Durban 4041, South Africa
[c] Department of Chemical Engineering, Indian Institute of Technology ((IIT) Kharagpur, India

ARTICLE INFO

Article history:
Received 30 June 2010
Received in revised form 4 November 2010
Accepted 30 December 2010
Available online 5 January 2011

Keywords:
Pollution control
Bubbling fluidized bed reactor
CO_2
Removal efficiency
Plug flow
Mixed flow

ABSTRACT

A bubbling counter-current multistage fluidized bed reactor for the sorption of carbon dioxide (CO_2) by hydrated lime particles was simulated employing a two-phase model, with the bubble phase assumed to be in plug flow, and the emulsion phase in plug flow and perfectly mixed flow conditions. To meet prescribed permissible limit to emit carbon dioxide from industrial flue gases, dry scrubbing of CO_2 was realized. For the evaluation, a pilot plant was built, on which also the removal efficiency of CO_2 was verified at different solids flow rates. The model results were compared with experimental data in terms of percentage removal efficiency of carbon dioxide. The comparison showed that the EGPF model agreed well with the experimental data satisfactorily. The removal efficiency was observed to be mainly influenced by flow rates of adsorbent and CO_2 concentration.

1. Introduction

Carbon dioxide in flue gas generated as a result of combustion of fossil fuel in, e.g., thermal power plants, etc., is the main cause of global environmental problems such as climate change. Many countries have therefore adopted stringent CO_2 emission standard for industries. The CO_2 emitting plants other than coal-fired thermal power plants comply with prescribed emission standard by wet processes resulting in generation of liquid effluent, which create more problems to handle with and dispose of. Since many inherent problems are associated with wet processes, the dry processes are now promoted to control the gaseous pollutants throughout the world. However, all the dry process techniques are mostly used in fixed bed or in single stage fluidized bed reactor at high temperature, which is not suitable for removal of carbon dioxide from flue gas in the industries. Thus the dry process to control CO_2 at lower temperature is the need of the day and the equipment to be selected for the control of carbon dioxide must have a very high efficiency of collection. Literature suggests that the fluidized bed reactor operating at various regimes can be used as possible equipment for removal of carbon dioxide at high temperature. But, at low temperature the efficiency of these reactors is very low besides other limitations. The limitations of a single stage continuous fluidized bed reactor can be avoided by the use of multistage continuous fluidized bed reactor due to its staging effects which, in turn, enhances separation efficiency. The gas–solid mass-transfer resistance in the fluidized bed reactor is so small that it can be neglected, and excellent temperature control is also achievable because of the vigorous mixing of solid particles in the bed [1]. This reactor has also the characteristics of low reaction temperature and sufficient reaction time, compared with the other reactor. In this paper a two-phase model has been developed for sorption of carbon dioxide on calcium hydroxide particles in a multistage fluidized bed reactor and simulation results are compared with experimental data.

2. Mathematical model

For normal operating velocities (3–8 times u_{mf}) the fluidized bed reactor can be approximated as a bubbling bed [2–3]. Bubbling fluidized beds have extensively been studied and variety of models of varying degree of complexity has been proposed in the literature [3–8]. Generally, for modeling of fluidized bed reactor either a two-phase model comprising of emulsion and bubble phases [3–7] or a three phase model comprising of an additional cloud phase is considered [8]. For Geldart B type particles, at higher values of u_g/u_{mf} ratio, the presence of cloud phase can be considered negligible [9]. The two phase model was used successfully applied for the drying of moist air by alumina particles in a counter-flow multi-

* Corresponding author. Tel.: +27 312603802; fax: +27 312601118.
E-mail address: meikap@ukzn.ac.za (B.C. Meikap).

0304-3894/$ – see front matter © 2011 Elsevier B.V. All rights reserved.
doi:10.1016/j.jhazmat.2010.12.122

Nomenclature

A	area of the reactor (m^2)
C_b	carbon dioxide concentration of bubbles (mol/m^3)
C_{bi}	carbon dioxide concentration of bubbles in ith stage (mol/m^3)
C_i	carbon dioxide concentration of gas leaving the ith stage (mol/m^3)
C_{i+1}	carbon dioxide concentration of gas entering the ith stage (mol/m^3)
C_{in}	carbon dioxide concentration of gas at the inlet (mol/m^3 or ppm)
C_{out}	carbon dioxide concentration of exit gas (mol/m^3 or ppm)
C_p	carbon dioxide concentration of emulsion phase (mol/m^3)
C_{pi}	carbon dioxide concentration of emulsion phase in ith stage (mol/m^3)
C_R	calcium hydroxide concentration of emulsion phase (mol/m^3)
C_{Ri}	calcium hydroxide concentration of emulsion phase in ith stage (mol/m^3)
C_{R_0}	calcium hydroxide concentration of emulsion phase entering (mol/m^3)
d_p	particle diameter (m)
F	fractional free area of distributor (%)
G_a	mass velocity of air (kg/m^2 s)
G_s	mass velocity of solids (kg/m^2 s)
g	acceleration due to gravity (m/s^2)
H	height of bed (m)
h_W	height of the weir (m)
k_1	reaction rate constant (m^3/mol s)
m_1, m_2	constants
N_b	number of bubbles per unit bed volume ($1/m^3$)
Q	inter-phase mass transfer flux (m^3/s)
r	average rate of CO_2 removal (mol/m^3 s)
u_g	superficial velocity of air (m/s)
u_s	superficial velocity of solids (m/s)
V_b	volume of bubble (m^3)
z	height in the bed (m)

Greek symbols

ρ_g	density of air (kg/m^3)
ρ_s	density of solids (kg/m^3)
ε_{mf}	bed voidage at minimum fluidization (–)
$(1-\varepsilon)$	fractional solids concentration (–)
β	fraction of gas flow associated with bubble phase (–)
η_{CO_2}	CO_2 removal efficiency (%)
ζ	solids mean residence time (s)

Subscripts

a/g	air/gas
b	bubbles
i	ith stage of column
$i+1$	$(i+1)$th stage of column
mf	minimum fluidization
p	particle
s	solids
e	experimental
c	calculated

stage fluidized bed reactor [10]. Therefore, it was decided to derive a model for the hydrodynamic behavior of gas for MFBR based on the assumptions with little modification [11]. The details of this model can be found elsewhere [12].

The mixing in a fluidized bed reactor is difficult to characterize, and in the literature both the phases (i.e., the emulsion and the bubbles) have been modeled either as a plug flow or perfectly mixed. The assumption of plug flow for the bubble phase is usually valid; however, it is not clear at all whether the emulsion phase should be modeled as being perfectly mixed or in plug flow. Literature suggests that the multistage fluidized bed reactor behave as a plug flow reactor. However, in the present study both flow regimes (plug and perfectly mixed) were considered for the emulsion phase together with plug flow regime for the bubble phase.

2.1. Kinetics

At low temperature, the primary reaction that has been traditionally proposed in the flue gas decarbonization process is as follows;

$$CaO(s) + CO_2(g) = CaCO_3(s) \quad (1)$$

Rate constant has been expressed according to Arrehenius' law:

$$k_1 = A_0 \exp\left(-\frac{E}{RT}\right) \quad (2)$$

where the activation energy of reaction is 38 kJ/mol, and for the pre-exponential factor we have $A_0 = 2.814\ m^3/mol\ s$ [13]

2.2. Model development

The assumptions made in developing the model for MFBR are summarized below:

1. The total bed consists of two phases (i) Solid-free bubble phase (ii) Solid-rich emulsion phase;
2. All gas in excess of that required for minimum fluidization passes through the bed as bubbles;
3. The bubble phase does not contain any solids;
4. The bubble phase is in plug flow and gas in bubbles is perfectly mixed;
5. The bubbles are spherical, of constant size and evenly distributed in the bed at any time;
6. As bubbles rise, bubbles exchange gas with rest of bed (emulsion phase). The inter-phase mass transfer results from two independent mechanism; bulk flow of gas and diffusion;
7. The mass transfer resistances between the particles and the dense phase gas are neglected;
8. The solid particles are perfectly mixed in emulsion phase (the emulsion phase is perfectly mixed), but gas in emulsion phase is considered (i) emulsion gas perfectly mixed (EGPM) model (ii) emulsion gas in plug flow (EGPF) model;

Additional assumptions;

1. Constant mean particle size is assumed through out bed;
2. Emulsion of solids at top of bed is neglected;
3. All the stages operate under same conditions of fluidization;
4. Holdup of solids is same on each stage;
5. All the particles entering first stage present the same concentration in active species;

So the assumptions lead in fact to two distinct models; (i) EGPF model (ii) EGPM model. Figs. 1 and 2 are the schematic of both the models.

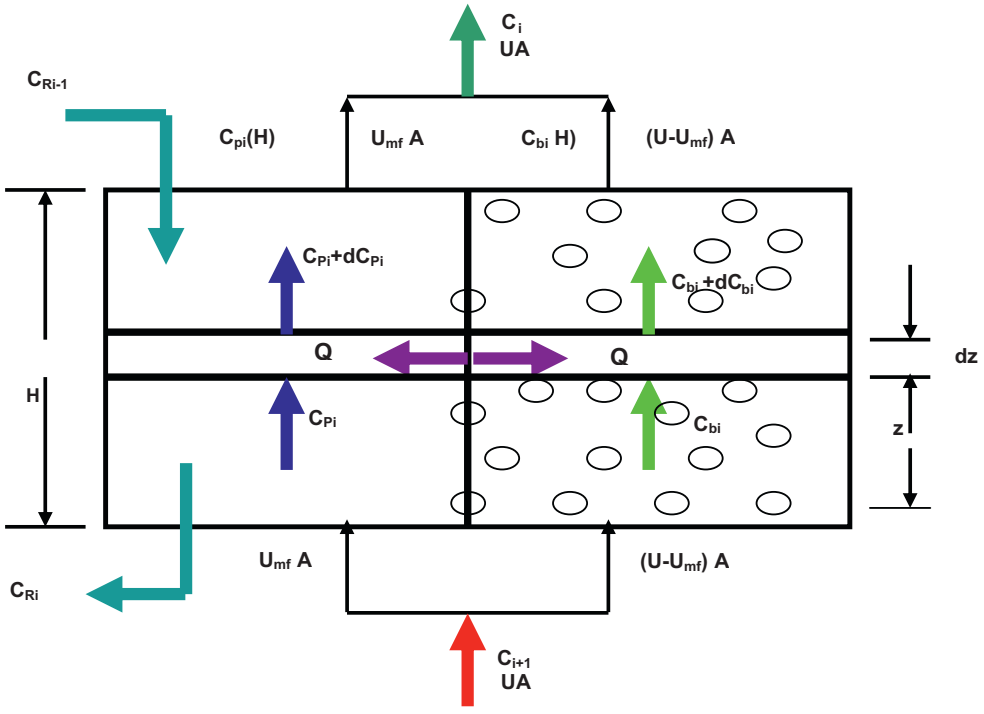

Fig. 1. Schematic of EGPF model.

2.3. Equations of the model

2.3.1. Mass balance at the exit

The mass balance for the reactant gas at the exit is

$$uC_i = u_{mf}C_{pi} + (u - u_{mf})C_{bi}(H) \quad (3)$$

Rearranging the terms, the concentration of gas leaving the ith stage,

$$C_i = \beta C_{bi}(H) + (1 - \beta)C_{pi} \quad (4)$$

where β is the fraction of gas flow associated to the bubble phase, i.e. $\beta = 1 - (u_{mf}/u)$.

2.3.2. Mass balance of carbon dioxide in bubble phase

The mass balance on carbon dioxide through the bubble phase of the ith stage is independent of the assumption relative to the behavior of gas in emulsion phase. Consider an element of thickness dz, at a height of z in bed, containing $N{\cdot}dz$ bubbles. The material balance is written for a unit horizontal cross sectional area by considering total bed height H. Combining the inlet and outlet terms and rearranging, it gives

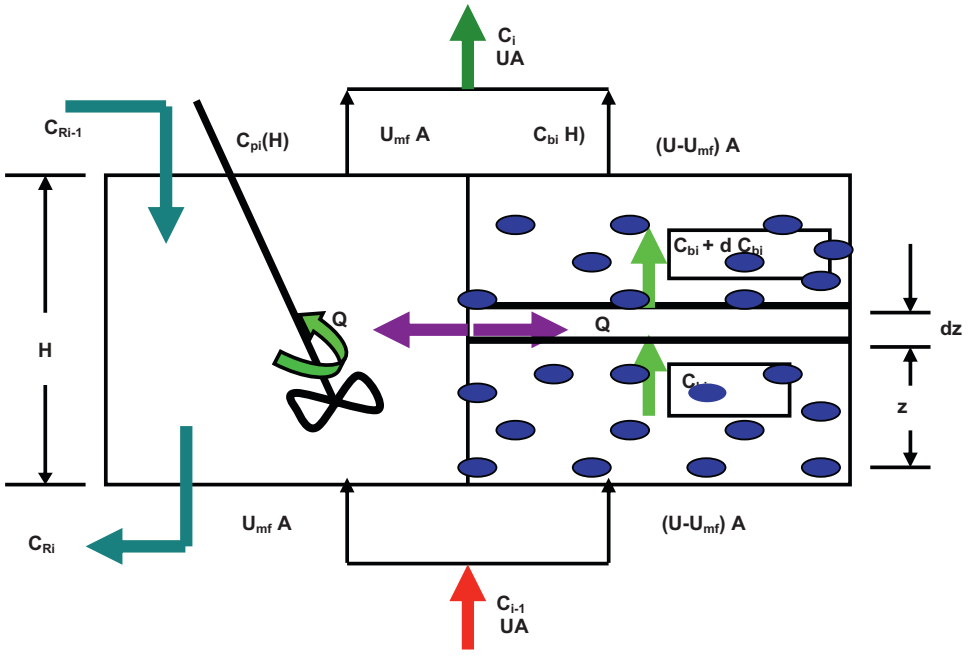

Fig. 2. Schematic of EGPM model.

Rate of change of reactant concentration = Loss of reactant by exchange

$$N_b Q(C_{pi} - dC_{bi}) = N_b V_b u_b \frac{dC_{bi}}{dz} \tag{5}$$

$$\frac{dC_{bi}}{dz}\left(\frac{V_b u_b}{Q}\right) = C_{pi} - C_{bi} \tag{6}$$

2.3.3. Emulsion phase

2.3.3.1. EGPM model. The material balance is written for unit horizontal cross sectional area by considering total bed height H. Combining inlet and outlet terms;

$$\int_0^H N_b Q C_{bi}\, dz + u_{mf} C_{i+1} = u_{mf} C_{pi} + C_{pi} \int_0^H N_b Q\, dz + \tilde{r} \int_0^H (1 - NV_b)\, dz \tag{7}$$

where the CO_2 concentration in the emulsion phase, C_{pi}, is independent of height z. H is the height of expanded bed assumed equal to height of the down comer over the distributor and $\tilde{r}$ is the average rate of disappearance of CO_2 in the entire emulsion phase.

2.3.3.2. EGPF model. Let us now consider that the gas is in plug flow through the emulsion phase with all same assumptions. The material balance over a unit cross-sectional area of dense phase considering an infinitesimal height dz;

$$u_{mf} C_{pi} + N_b Q C_{bi}\, dz = u_{mf}(C_{pi} + dC_{pi}) + N_b Q C_{pi}\, dz + r_i(1 - N_b V) dz \tag{8}$$

Rearranging the term, we get

$$u_{mf} \frac{dC_{pi}}{dz} + N_b Q(C_{pi} - C_{bi}) + K_1 C_{pi}(1 - N_b V) dz = 0 \tag{9}$$

where the CO_2 concentration in the emulsion phase, C_{pi}, and $\tilde{r}$ are functions of z.

2.3.4. Mass balance on the sorbent particles

At any time over the ith stage, the disappearance rate of calcium oxide (R) according to the rate kinetics can be written as:

$$\frac{\partial C_{Ri}}{\partial t} = -k_1 C_{Ri} C_{pi} \tag{10}$$

2.3.4.1. EGPM model. The calcium hydroxide concentration is

$$C_{Ri} = C_{Ri_0} \exp(-k_1 C_{pi} \overline{\tau_i}) \tag{11}$$

where $\overline{\tau_i}$ is mean residence time of solids in each stage.

Which can be expressed as the function of initial concentration of sorbent, C_{R_0} of the particles entering the first stage of the reactor:

$$C_{Ri} = C_{R_0} \exp(-k_1 \sum C_{pj} \overline{\tau_j}) \quad \text{for} \quad j = 1 \quad \text{to} \quad i \tag{12}$$

2.3.4.2. EGPF model. The carbon dioxide concentration of gas varies throughout the emulsion phase, but the solid particles which are perfectly mixed, have at any time, an equal probability of contacting an element of gas volume, whose concentration C_{pi} lies between C_{i+1} and $C_{pi}(H)$. Therefore, it can be accepted that considering all the particles, the carbon dioxide concentration of gas is $\overline{C_{pi}}$ which is defined by the equation

$$\overline{C_{pi}} = \frac{1}{H} \int_0^H C_{pi}\, dz \tag{13}$$

2.3.5. Carbon dioxide concentration in the exit gas stream from ith stage

The rate of CO_2 disappearance in ith stage can be expressed as

$$r_i = (k_1 \overline{C_{Ri}}) C_{pi} \tag{14}$$

The term in the bracket remains constant over the entire emulsion phase so that the reaction rate can be considered as first order, i.e.

$$r_i = (k_1 \overline{C_{Ri}}) C_{pi} = k C_{pi} \tag{15}$$

2.3.6. Analytical solution of model equation

2.3.6.1. Bubble phase. Integrating the Eq. (6) from 0 to H with boundary condition at $z = 0$, $C_{bi} = C_{i+1}$ and $z = H$, $C_{bi} = C_{bi}(H)$

$$\int_0^H \frac{dC_{bi}}{C_{pi} - C_{bi}} = \int_0^H \left(\frac{Q}{V_b u_b}\right) dz \tag{16}$$

$$C_{bi}(z) = C_{pi} + (C_{i+1} - C_{pi}) e^{Qz/u_b V_b} \tag{17}$$

$$C_{bi}(H) = C_{pi} + (C_{i+1} - C_{pi}) e^{-X} \tag{18}$$

where $X = (QH/u_b V_b)$ indicates the number of times a bubble is purged as it rises through the bed or number of times the gas within the bubble is exchanged with the particulate phase during the passage through the bed.

2.3.6.2. EGPM model. Rearranging the terms of the Eq. (7) and simplifying, the equation is;

$$u_{mf}(C_{i+1} - C_{pi}) = N_b Q \int_0^H (C_{pi} - C_{bi}) dz + \tilde{r} \int_0^H (1 - NV_b) dz \tag{19}$$

Eliminating C_{pi} from RHS of the Eq. (19), the equation is

$$u_{mf}(C_{i+1} - C_{pi}) = N_b u_b V_b \int_0^H dC_{bi} + \tilde{r} \int_0^H (1 - NV_b) dz \tag{20}$$

Integrating the Eq. (20) from 0 to H with boundary condition at $z = 0$, $C_{bi} = C_{i+1}$ and $z = H$, $C_{bi} = C_{bi}(H)$

$$u_{mf}(C_{i+1} - C_{pi}) = N_b u_b V_b \{C_{bi}(H) - C_{i+1}\} + k C_{pi}(1 - NV_b) H \tag{21}$$

Putting the value of $C_{bi}(H)$ in the Eq. (21) and rearranging, we get

$$C_{pi} = \frac{C_{i+1}(1 - \beta e^{-X})}{1 - \beta e^{-X} + (KH_{mf}/u)} \tag{22}$$

$$C_{bi}(H) = C_{pi} + (C_{i+1} - C_{pi}) e^{-X} \tag{23}$$

Putting the above values of C_{pi} and $C_{bi}(H)$ in the Eq. (4), it gives the CO_2 exit concentration from ith stage for the model.

2.3.6.3. EGPF model. Eliminating C_{pi} from the Eq. (9) and expressing the equation in terms of C_{bi},

$$\frac{d^2 C_{bi}}{dz^2} + \frac{u_{mf}\{1 + (d/dz)(u_b V_b/Q)\} + N_b u_b V_b + K_1(1 - N_b V_b)(u_b V_b/Q)}{u_b V_b u_{mf}/Q} \frac{dC_{bi}}{dz} + \frac{K_1(1 - N_b V_b)}{u_b V_b u_{mf}/Q} C_{bi} = 0 \tag{24}$$

Let us assume

$$a = \frac{u_{mf}\{1 + (d/dz)(u_b V_b/Q)\} + N_b u_b V_b + K_1(1 - N_b V_b)(u_b V_b/Q)}{u_b V_b u_{mf}/Q} \tag{25}$$

and

$$b = \frac{K_1(1 - N_b V_b)}{u_b V_b u_{mf}/Q} \tag{26}$$

Now the Eq. (24) is $(d^2 C_{bi}/dz^2) + a(dC_{bi}/dz) + bC_{bi} = 0$ is a second order differential equation with respect to C_{bi}. Now the equation can be written as

$$(D^2 + aD + b) C_{bi} = 0 \tag{27}$$

The auxiliary equation is

$$m^2 + am + b = 0 \tag{28}$$

Table 1
Hydrodynamic and transport property correlations.

Parameter	Correlation	Reference
Bubble diameter	$D_b(Z) = D_{b\max} - (D_{b\max} - D_{b_0})\exp\left(\frac{-0.3z}{D_T}\right)$	[13]
Bubble velocity	$u_b = u_0 - u_{mf} + u_{br}$	[13]
Bubble rise velocity	$u_{br} = 0.711(gD_b)^{0.5}$	[13]
Emulsion phase volumetric flow rate	$Q_e = u_{mf}A$	[13]
Bubble phase volumetric flow rate	$Q_b = (u - u_{mf})A$	[13]
Height of bed at rest	$H_{mf} = H(1 - N_b V_b) = H\left(1 - \frac{u-u_{mf}}{u_b}\right)$	[13]
Interphase mass transfer	$Q = \left[\frac{3}{4}u_{mf} + 0.975D_G^{0.5}\left(\frac{g}{D_b}\right)^{0.25}\right]\pi D_b^2$	[13]
Number of bubbles per unit bed volume	$N_b = \frac{u-u_{mf}}{V_b u_b}$	[13]
Bubble volume	$V_b = \frac{\pi D_b^3}{6}$	[13]
Diameter of reactor	$D_T = 0.1$ m	
Diffusivity of gaseous reactant	$D_g(T) = 8.0 \times 10^{-26} T^{7.5}$	[13]

Since this is a quadratic equation, the characteristic roots of the equation are m_1 and m_2, then complementary functions of the equation

$$C_{bi} = c_1 e^{m_1 z} + c_2 e^{m_2 z} \tag{29}$$

The above equation can be solved by following boundary equations;

$$\text{At} \quad z = 0, \quad C_{bi} = C_{i+1} \quad \text{and} \quad \frac{dC_{bi}}{dz} = 0$$

$$\text{At} \quad z = H, \quad C_{bi} = C_{bi}(H)$$

Differentiating the Eq. (29), we get

$$\frac{dC_{bi}}{dz} = c_1 m_1 e^{m_1 z} + c_2 m_2 e^{m_2 z} \tag{30}$$

At $z = 0$, the equation becomes,

$$C_{bi} = C_{i+1} = c_1 + c_2 \quad \text{and} \quad c_1 m_1 + c_2 m_2 = 0 \tag{31}$$

At $z = H$, the equation is

$$C_{bi}(H) = c_1 e^{m_1 H} + c_2 e^{m_2 H} \tag{32}$$

Solving the Eqs. (31) and (32), we get

$$c_1 = \frac{-m_2 C_{i+1}}{m_1 - m_2} \tag{33}$$

$$c_2 = \frac{m_1 C_{i+1}}{m_1 - m_2} \tag{34}$$

Putting the value of c_1, c_2 in the Eq. (32), the equation becomes

$$C_{bi}(H) = \frac{C_{i+1}}{m_1 - m_2} m_1 e^{m_2 H} - m_2 e^{m_1 H} \tag{35}$$

Putting the value of C_{bi} in the Eq. (18), we get

$$C_{pi} = \left(\frac{C_{i+1}}{m_1 - m_2}\right)\left[m_{1i}\left(1 + \frac{H}{X}m_2\right)\exp(m_2 H) - m_2\left(1 + \frac{H}{X}m_1\right)\exp(m_1 H)\right] \tag{36}$$

Putting the values and solving a and b, these become,

$$a = \frac{X + K}{(1 - \beta)H} \tag{37}$$

$$b = \frac{K.X}{(1 - \beta)H^2} \tag{38}$$

where K_i is the number of reaction unit in emulsion phase

$$K_i = KC_{Ri}\frac{H_{mf}}{U} \tag{39}$$

Putting the values of a and b in the auxiliary Eq. (28), the equation becomes

$$H(1 - \beta)m^2 - (X + K)m + \frac{XK}{H} = 0 \tag{40}$$

Then the roots of the equation are

$$m_{1\,\text{or}\,2} = \frac{1}{2}\frac{X + K}{H(1 - \beta)} \pm \frac{1}{2}\left[\left(\frac{X + K}{H(1 - \beta)}\right)^2 - 4\frac{XK}{H^2(1 - \beta)}\right] \tag{41}$$

For ith stage

$$m_{1i\,\text{or}\,2i} = \frac{1}{2}\frac{X + K_i}{H(1 - \beta)} \pm \frac{1}{2}\left[\left(\frac{X + K_i}{H(1 - \beta)}\right)^2 - 4\frac{XK_i}{H^2(1 - \beta)}\right] \tag{42}$$

$$C_{bi}(H) = \frac{C_{i+1}}{m_{1i} - m_{2i}} m_{1i} e^{m_{2i} H} - m_{2i} e^{m_{1i} H} \tag{43}$$

$$C_{pi} = \left(\frac{C_{i+1}}{m_{1i} - m_{2i}}\right)\left[m_{1i}\left(1 + \frac{H}{X}m_{2i}\right)\exp(m_{2i}H) - m_{2i}\left(1 + \frac{H}{X}m_{1i}\right)\exp(m_{1i}H)\right] \tag{44}$$

Mean concentration of emulsion gas is given by

$$C_{pi} = \frac{1}{H}\left(\frac{C_{i+1}}{m_{1i} - m_{2i}}\right)\left[\frac{m_{1i}}{m_{2i}}\left(1 + \frac{H}{X}m_{2i}\right)[\exp(m_{2i}H) - 1] - \frac{m_{2i}}{m_{1i}}\left(1 + \frac{H}{X}m_{1i}\right)[\exp(m_{1i}H) - 1]\right] \tag{45}$$

Putting the above values of C_{pi} and $C_{bi}(H)$ in the Eq. (4), it gives the CO_2 exit concentration from ith stage for the model.

2.4. Estimation of hydrodynamic parameters

In order to solve the set of equations, it is necessary to relate several parameters appearing in these equations, including the bubble volume fraction, the bubble size, the inter-phase mass and heat transfer coefficients, to the design and operating parameters. Correct evaluation of these parameters is crucial for the accurate simulation of the operation of an industrial fluidized bed reactor. Several empirical correlations have been proposed for estimating these parameters. For the purpose of this study, an illustrative set was chosen. This set of hydrodynamic correlations is given in Table 1.

3. Experimental technique and procedure

Fig. 3 is the schematic of the multi-stage fluidized bed reactor developed and used in this study. The configuration of this staged gas–solid fluidized bed reactor is similar to that of the sieve trays

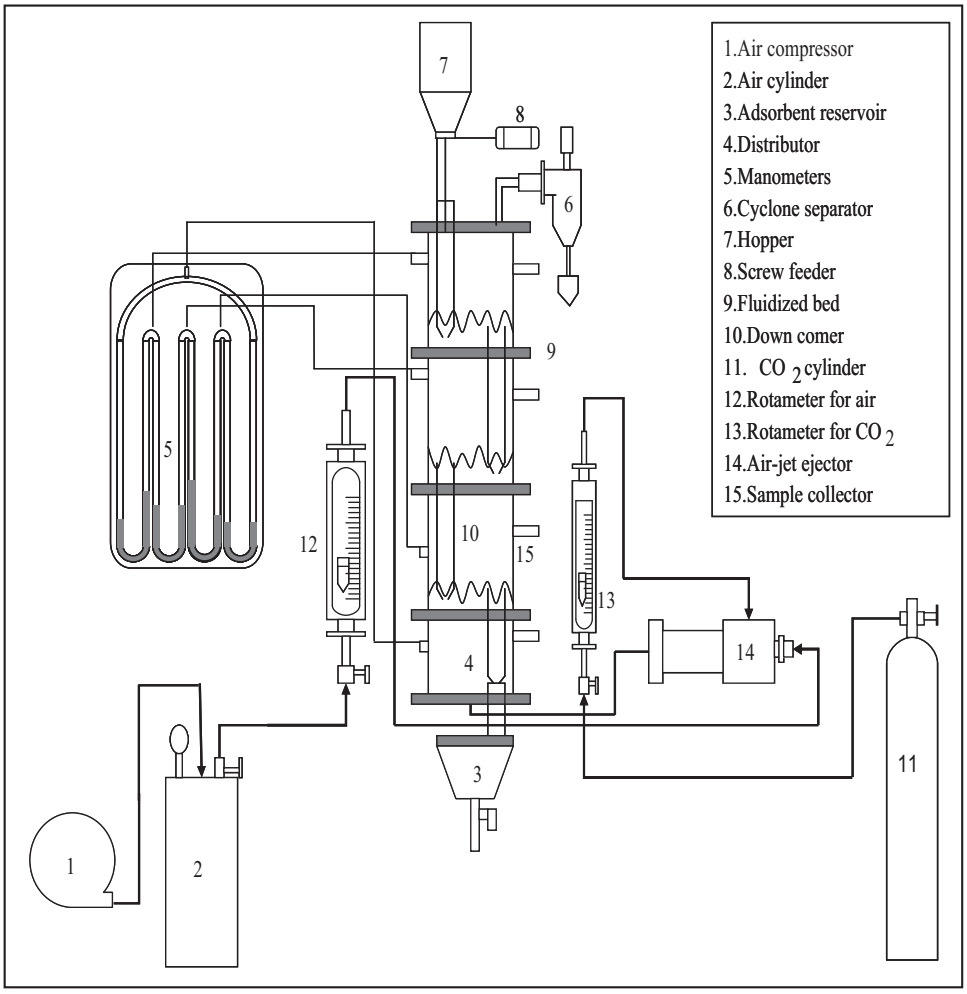

Fig. 3. Schematic diagram of the experimental set-up of a three-stage gas–solid fluidized bed reactor.

distillation column. The reactor consisted of a three stage fluidization column having provision of solid and air feeding from the top and bottom, respectively, along with other auxiliary equipments used for experimentation. Each stage of the column was made up of Perspex cylinder of 0.10 m internal diameter and 0.305 m long. The stainless steel plates were used as internal baffles sandwiched between the flanges of two stages and each plate was drilled with perforations having 8.56% total grid openings [14]. The grid plates were fixed with fine wire mesh (100 mesh size) to prevent weeping of the solid particles through the openings. Each section was provided with a downcomer of Perspex cylinder of 0.025 m internal diameter and the downcomers were fitted to the gas distributor by special threading arrangement having the provision for adjusting the weir height as desired. The downcomers were further fitted with a cone at the exit end in order to reduce the up flow of the gas through the downcomer and consequently, widening the stable operating range. Pressure tapings were provided just below the grid plate and the near the air out let and was provided with weir mesh filter to prevent any solid particle from the entering the tapings. Four manometers were provided to measure the pressure drop at every stage as well as the total pressure drop.

In order to generate synthetic air–CO_2 mixture, in composition similar to that of the exhaust of carbonic acid plants, cupper smelters was made by mixing compressed air from an air compressor and CO_2 gas from an CO_2 cylinder. Provision was made to feed the air–CO_2 mixture at the base of the fluidized bed reactor. The air–CO_2 mixture was generated by mixing air and CO_2 in an air-jet ejector assembly. Compressed air from the compressor was used as the motive fluid in the ejector to aspirate and thoroughly mix air with CO_2 from the CO_2 gas cylinder. The ejector was mounted with a downward slope of 30° with an air nozzle perfectly aligned along the axis of the ejector throat to ensure an axially symmetrical jet. The air nozzle was fixed at a projection ratio (which is the ratio of the distance between the nozzle tip and the beginning of

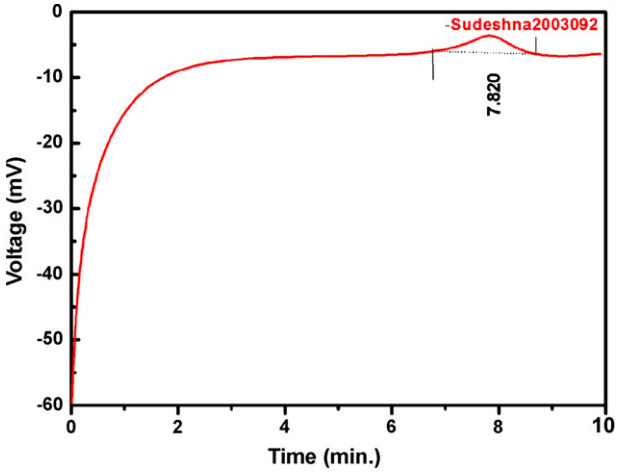

Fig. 4. Calibration curve for pure CO_2.

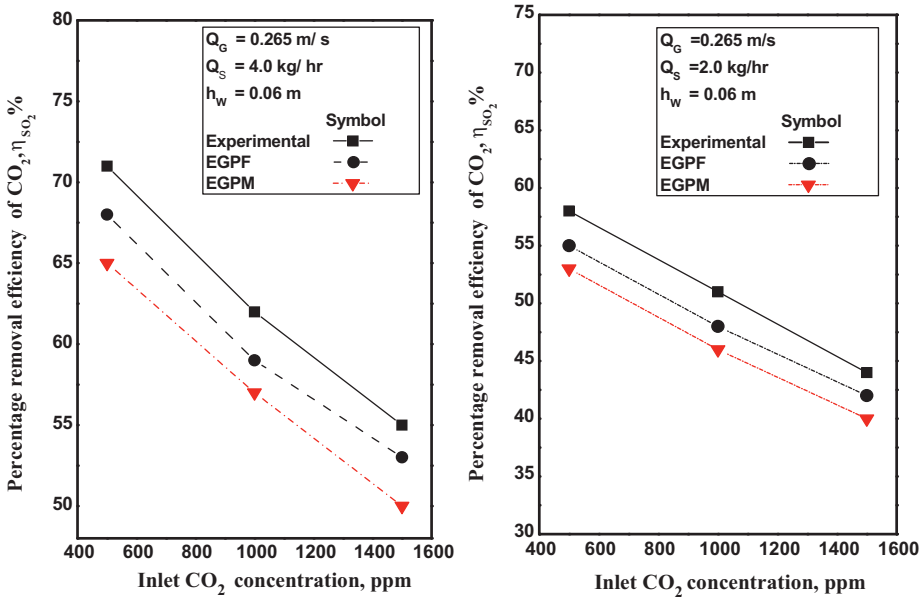

Fig. 5. Effect of inlet CO_2 concentration on percentage removal efficiency of CO_2 at h_W = 0.06 m.

Table 2
Characteristics of hydrated lime.

Adsorbent	Characteristic	Value
Hydrated lime	Average particle diameter (μm)	426
	Density (kg/m^3)	2040
	Minimum fluidization velocity (m/s)	0.112
	Specific area of unreacted sorbent (m^2/g)	15
	Average pore diameter (Å)	98.4
	Pore volume (cm^3/g)	1.213

the parallel throat to the throat diameter), of 3.78, which was determined experimentally for obtaining the highest possible mass ratio of aspirated gas. Compressed air at the desired pressure and flow rate was forced through the air nozzle and regulated by a valve. Simultaneously the CO_2 was routed at a controlled rate through CO_2 gas regulator and into the ejector. The air–CO_2 gas mixed intensely in the mixing throat of the ejector and the mixture was fed into pre-distributor fitted at the bottom of the column. Pre-calibrated rotameter were used to measure the gas flow rate.

Table 3
Chemical composition of hydrated lime.

Compound	Weight (%)
CaO	25.0
$Ca(OH)_2$	64.4
$CaCO_3$	4.76
MgO	3.22
Impurities	2.62

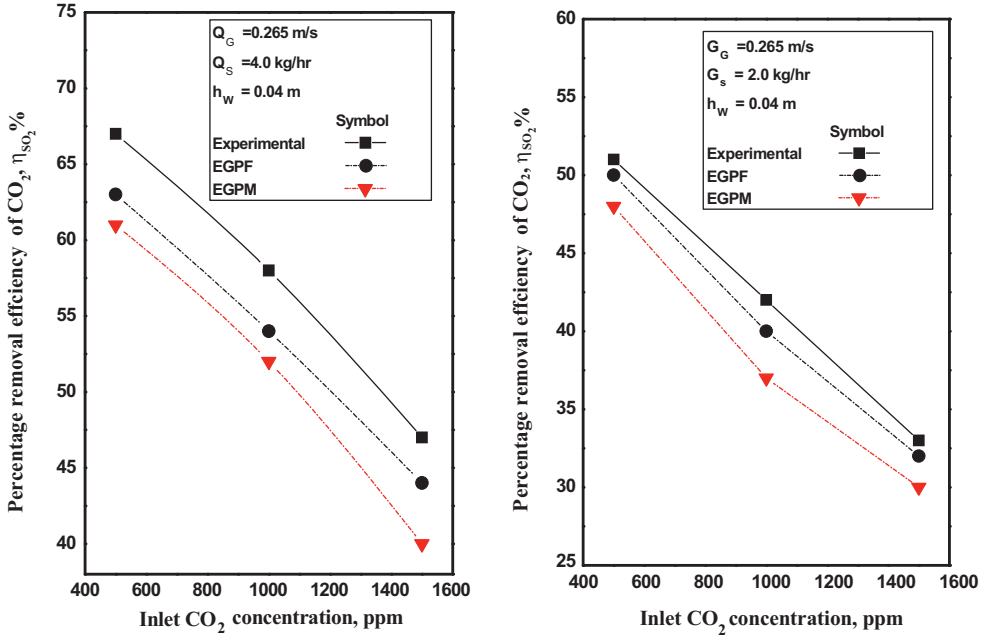

Fig. 6. Effect of inlet CO_2 concentration on percentage removal efficiency of CO_2 at h_W = 0.04 m.

A conical hopper was attached at the bottom of column for storage of solids coming out from the bottom stage through the downcomer. The gas leaving the column from the top stage was passed through a standard cyclone and then into the exhaust system.

The solids from the screw feeder were fed to the first stage downcomer of the reactor. Necessary precautions were made to ensure that no air from outside intruded into the column during operation.

Tables 2 and 3 show the physical and chemical characteristic of hydrated lime considered for the study. The gas velocity was set at 0.265 m/s (31.2×10^{-2} kg/m^2 s). The solid flow rates were 2 kg/h (71.0×10^{-3} kg/m^2 s) and 4 kg/h (141.5×10^{-3} kg/m^2 s). The weir height of the down-comer was kept at 40 mm and 60 mm and the gap between the down-comer bottom and the grid plate were kept 20 mm and 30 mm, respectively. For each gas velocity the inlet CO_2 concentration was varied between 500 ppm to 1500 ppm. The experiments were carried out at a pressure of 1 atm and at room temperature. The percentage removal of CO_2 has been calculated for each experimental run by the formula given below:

$$\eta_{CO_2} = \frac{CO_{2,\text{inlet}} - CO_{2,\text{outlet}}}{CO_{2,\text{inlet}}} \times 100 \quad (46)$$

Similarly for ith stage,

$$\eta_{CO_2} = \frac{C_{i+1} - C_i}{C_{i+1}} \quad (47)$$

where C_i = outlet CO_2 concentration in the gas; C_{i+1} = inlet CO_2 concentration in the gas.

In this study, the effects of the superficial gas velocity, superficial solid velocity and weir height on the removal efficiency of CO_2 was investigated.

3.1. Sampling and analysis

Prior to sampling of the gas, the reactor was operated for quite some time until all the stages of the reactor were identical in their operation and the pressure drops across each stage was almost equal indicating steady and stable operation of the reactor. The steady state condition in the reactor occurred when material inflow into the system and outflow of bed material from the system were found to be almost same. Samples at the inlet and outlet of the column were drawn with the help of syringes, and these CO_2 gas samples were analyzed in the gas chromatograph (GC). Fig. 4 represents the calibration curve obtained in GC for pure CO_2. The other samples were analyzed, and the areas under the curves were compared. From that, the percentage of CO_2 in the samples was calculated. The range of the concentration of CO_2 monitoring was 500–1500 ppm, and the accuracy was 10 ppm.

4. Results and discussion

The concentration of the gas stream exiting each stage has been calculated by solving the equation of the models. The calcium hydroxide concentration (C_{R_0}) of the sorbent particles entering the reactor, expressed in moles of calcium hydroxide per unit volume of solids, was determined by analysis. To solve the equations, a simulation program is developed in Matlab and based on the program following result have been obtained and compared with experimental values.

4.1. Effect of inlet concentration on carbon dioxide removal efficiency

Fig. 5 represents the effect of different inlet carbon dioxide loading on the percentage removal of CO_2 at a particular mass velocity of gas (31.2×10^{-2} kg/m^2 s) and weir height 60 mm. For this set of prediction, temperature was set to 310 K. It may be observed that the removal efficiency decreases as the inlet carbon dioxide concentration increases. The percentage removal of CO_2 is higher for EGPF model compared to EGPM model. The percentage removal of carbon dioxide is 68% for EGPF model and 65% for EGPM model for 500 ppm inlet concentration at 60 mm weir height and mass velocity of solids (141.5×10^{-3} kg/m^2 s). For same inlet concentration and weir height, the percentage of carbon dioxide removal is 55% for EGPF model and 53% for EGPM model at mass velocity of solids (71.0×10^{-3} kg/m^2 s). It indicates that decreasing in the mass velocity of solids decreases the removal efficiency, as the probability of collision between gas and solid particles decreases due to decrease in solids holdup.

Fig. 6 represents the effect of inlet carbon dioxide concentration on the percentage removal of CO_2 at a particular mass velocity of gas 31.2×10^{-2} kg/m^2 s and weir height 30 mm. Similar trends have been emerged. The percentage removal of CO_2 is also higher for EGPF model. The percentage removal efficiency of carbon dioxide is 63% for EGPF model and 61% for EGPM model for 500 ppm inlet concentration at mass velocity of solids (141.5×10^{-3} kg/m^2 s). The percentage of carbon dioxide is 50% for EGPF model and 48% for EGPM model for same inlet concentration and weir height at mass velocity of solids (71.0×10^{-3} kg/m^2 s). It indicates that decreasing in the weir height decreases the removal efficiency, as the solids holdup in the bed decreases.

It may also be observed that a higher solid flow rate (141.5×10^{-3} kg/m^2 s) at a particular gas velocity has higher carbon dioxide removal efficiency than lower solid flow rate (71.0×10^{-3} kg/m^2 s) for both models.

5. Conclusions

A model based on assumption of Davison and Harrison with little modification has been developed for simulating the operation of reactor. The assumption of plug flow of the gas percolating through the emulsion phase leads to slightly better prediction than the assumption of perfect mixing of the emulsion phase. Based on prediction, it can be showed that with increase in mass velocity of solids, and weir height increase carbon dioxide removal efficiency. Maximum CO_2 was removed in first stage of the reactor. Increase in inlet concentration of carbon dioxide decreased removal efficiency.

Even though the some of conclusions are specific to the study, the model could be considered general enough to be used for predicting the performance of a counter-current multistage fluidized bed reactor for gas–solid treatment.

References

[1] M.H. Khani, H. Pahlavanzadeh, M. Ghannadi, Two-phase modeling of a gas phase fluidized bed reactor for the fluorination of uranium tetrafluoride, Ann. Nucl. Energy 35 (2008) 704–707.
[2] H.P. Cui, N. Mostuofi, J. Chaoki, Characterization of dynamic gas–solid distribution in the fluidized beds, Chem. Eng. J. 79 (2000) 135–141.
[3] K.B. McAuley, J.P. Talbot, T.J. Harris, A comparison of two phase and well-mixed models for fluidized-bed polyethylene reactor, Chem. Eng. Sci. 49 (1994) 2035–2045.
[4] D.K. Ghosh, Studies on the desulphurization of flue gas by porous solid reactants, Ph.D. Thesis, Indian Institute of Technology, Kharagpur, India, 1987.
[5] K. Hymore, C. Laguerie, Analysis and modeling of the operation of a counter-flow multistage fluidized bed adsorber for drying moist air, Chem. Eng. Process. 18 (1984) 255–267.
[6] Y.M. Harshe, R.P. Utikar, V.V. Ranade, A computational model for predicting particle size distribution and performance of fluidized bed polypropylene reactor, Chem. Eng. Sci. 59 (2004) 5145–5156.
[7] S. Mori, C.Y. Wen, Estimation of bubble diameter in gaseous fluidized beds, AIChE J. 21 (1975) 109–115.
[8] J.F. Davidson, D. Harrison, Fluidized Particles, Cambridge University Press, Cambridge, UK, 1963.

[9] W.Z. Lu, L.H. Teng, W.D. Xiao, Simulation and experiment study of dimethyl ether synthesis from syngas in a fluidized-bed reactor, Chem. Eng. Sci. 59 (2004) 5455–5464.
[10] J.Y. Kim, K.Y. Choi, Polymer particle mixing and segregation in a gas phase olefin polymerization reactor, AIChE Symp. Ser. 95 (1999) 77–81.
[11] H. Hatzantonis, H. Yiannoulakis, A. Yiagopoulos, C. Kiparissides, Recent developments in modeling gas-phase catalyzed olefin polymerization fluidized bed reactors: The effect of bubble size variation on the reactor's performance, Chem. Eng. Sci. 55 (2000) 3237–3259.
[12] D. Kunii, O. Levenspiel, Fluidization Engineering, 2nd ed., Butterworth-Heinemann, Boston, MA, 1991.
[13] A. Kiashemshaki, N. Mostoufi, R. Sotudeh-Gharebagh, Two-phase modeling of a gas phase polyethylene fluidized bed reactor, Chem. Eng. Sci. 61 (2000) 3997–4006.
[14] R.E. Treybal, Mass Transfer Operations, 3rd ed., McGraw-Hill, New York, 1980.